LANGMUIR Article
Cite This: Langmuir 2019, 35, 5013−5020
pubs.acs.org/Langmuir

Modeling the Cooperative Adsorption of Solid-Binding Proteins on Silica: Molecular Insights from Surface Plasmon Resonance Measurements

Brittney Hellner, Seong Beom Lee, Akshay Subramaniam, Venkat R. Subramanian, and François Baneyx*

Department of Chemical Engineering, University of Washington, Box 351750 Seattle, 98195 Washington, United States

Supporting Information

ABSTRACT: Combinatorially selected solid-binding peptides (SBPs) provide a versatile route for synthesizing advanced materials and devices, especially when they are installed within structurally or functionally useful protein scaffolds. However, their promise has not been fully realized because we lack a predictive understanding of SBP-material interactions. Thermodynamic and kinetic binding parameters obtained by fitting quartz crystal microbalance and surface plasmon resonance (SPR) data with the Langmuir model whose assumptions are rarely satisfied provide limited information on underpinning molecular interactions. Using SPR, we show here that a technologically useful SBP called Car9 confers proteins to which is fused a sigmoidal adsorption behavior modulated by partner identity, quaternary structure, and ionic strength. We develop a two-step cooperative model that accurately captures the kinetics of silica binding and provides insights into how SBP−SBP interactions, fused scaffold, and solution conditions modulate adsorption. Because cooperative binding can be converted to Langmuir adhesion by mutagenesis, our approach offers a path to identify and to better understand and design practically useful SBPs.

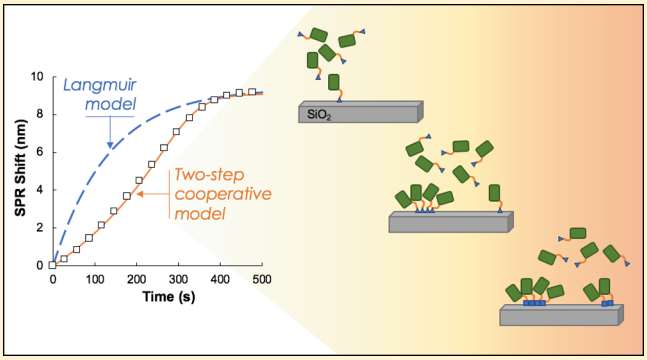

INTRODUCTION

Whether derived from biomineralizing organisms or identified by phage or cell surface display, solid-binding peptides (SBPs, a.k.a. material-binding peptides) provide a rich source of synthetic or genetically encodable chemistry to control the structure, composition, and properties of advanced materials and devices.[1−3] Applications are numerous and range from biomedical engineering[4−7] to catalysis[8,9] and from energy materials[10−12] to opto-electronics.[13,14] However, despite many success stories and progress in characterization and simulation, we remain unable to replicate nature's exquisite degree of control over inorganic morphogenesis and assembly in part because our understanding of how SBPs interact with surfaces remains limited.

Experimental tools to probe the biotic−abiotic interaction include quartz crystal microbalance (QCM), surface plasmon resonance (SPR), sum frequency generation, solid-state nuclear magnetic resonance, and atomic force microscopy (AFM).[15−22] Among these techniques, QCM, SPR, and AFM can provide kinetic and thermodynamic information but SPR is particularly attractive because it rapidly and accurately quantifies binding kinetics by monitoring how the refractive index changes over time when an analyte binds to a gold surface coated with a target ligand or material.[23,24] While SPR has been extensively used to characterize the binding of biomacromolecules to immobilized ligands, lipid bilayers, polymer films, and other biomaterials,[25] it has seldom been employed to monitor the interaction of SBPs with inorganic surfaces.[21,26−31] Furthermore, these studies have primarily focused on gold and platinum interfaces and employed 1:1 Langmuir binding or two-state reaction models that do not consider the complex protein−protein interactions that modulate surface recognition.[32]

Car9 is a SBP of amino acid sequence DSARGFKKPGKR that binds to the hydroxyl-, carbonyl-, and carboxylate-rich edges of graphitic nanostructures and exhibits a preference for sp^3-hybridized carbon.[31] Following its original identification as a carbon-binding peptide, Car9 has been found to bind to silica,[33] enabling the creation of hybrid architectures,[34] and the affinity purification,[33,35] immobilization,[36] and microcontact printing[37] of proteins to which it is fused.

While using SPR to quantify the binding of sfGFP−Car9 (a fusion between superfolder green fluorescent protein[38] and the Car9 SBP) to silica-coated gold chips, we observed an unusual sigmoidal adsorption behavior. Here, we describe the construction and validation of a two-step cooperative model

Received: January 30, 2019
Revised: March 6, 2019
Published: March 14, 2019

DOI: 10.1021/acs.langmuir.9b00283
Langmuir 2019, 35, 5013−5020

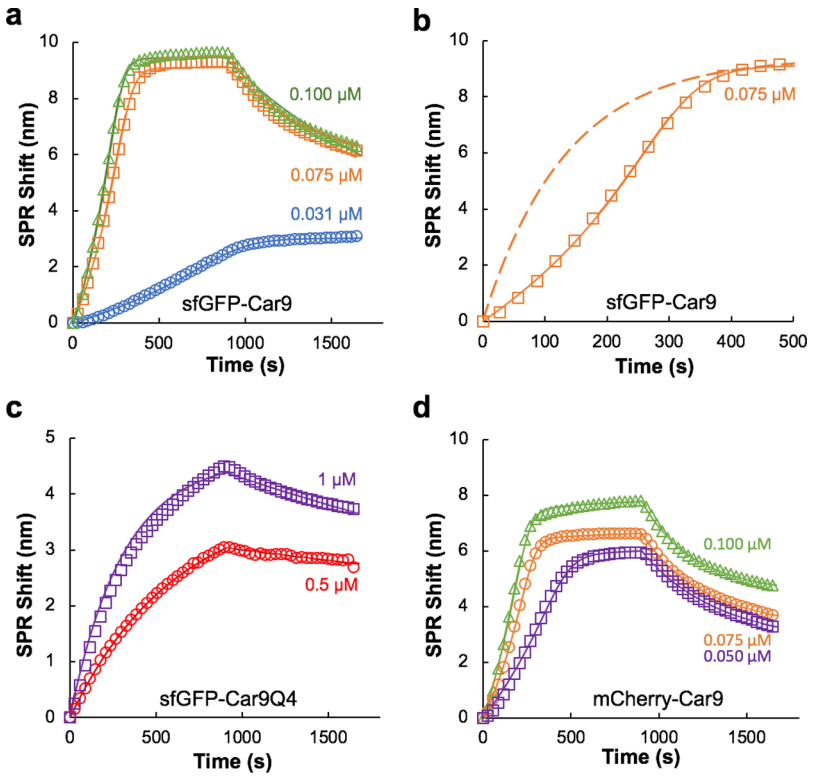

Figure 1. Adsorption kinetics of sfGFP−Car9 (a,b), sfGFP−Car9Q4 (c), and mCherry−Car9 (d) on silica-coated SPR chips. Sensorgrams were collected using the indicated protein concentrations. A wash phase in which protein-free buffer is flowed over the chip starts at t = 900 s and causes protein desorption. In panel (b), fitting of the sfGFP−Car9 adsorption phase with a kinetic Langmuir model is denoted with a dashed orange line while the fit obtained with the two-step cooperative adsorption model is shown with a solid orange line. The SPR shift is plotted on a different scale and higher protein concentrations are used in panel (c). All solid lines in panels (a,d) were obtained by fitting experimental data to the two-step cooperative adsorption model. All solid lines in panel (c) were obtained by fitting experimental data to a rate law-based Langmuir model. See text for details.

that captures the silica binding kinetics of sfGFP−Car9 and other Car9 fusion proteins with high fidelity. We further show that extracted model parameters deliver insights into the complex interplay between the surface, SBPs, fused framework, and ions, which should improve our ability to design solid-binding proteins for practical applications and predictive material synthesis.

EXPERIMENTAL SECTION

DNA Manipulations and Protein Purification. Plasmid pET-24a(+)-sfGFP−Car9 was described elsewhere.[33] Plasmid pET-24a(+)-nh-mCherry−Car9, which encodes a mCherry−Car9 fusion protein with an unmodified N-terminus, was constructed by polymerase chain reaction (PCR) amplification of this segment from pET-24a(+)-mCherry−Car9[33] and ligation into the *Nde*I and *Xho*I sites of pET-24a(+). Plasmid pET-24a(+)-sfGFP−Car9Q4, which encodes a fusion between sfGFP and Car9Q4 (DSARGFQQPGQQ) with an intervening GGGS linker, was obtained by inserting a DNA cassette encoding these elements between the *Hin*dIII and *Xho*I sites of pET-24a(+)-sfGFP−Car9. To create plasmid pET-24a(+)-GK−Car9 which encodes a fusion between GK and Car9 with a GGGS linker, a DNA fragment coding for glucose hexokinase (GK) and flanked by *Nde*I and *Hin*dIII sites, was PCR-amplified from *Geobacillus stearothermophilus* DNA and inserted into the same sites of pET-24a(+)-sfGFP−Car9. All constructs were verified by DNA sequencing. Proteins were expressed and purified by silica-affinity chromatography as described,[33,35] and the buffer was exchanged to 20 mM Tris-HCl at pH 7.5 by dialysis. Concentrations were determined by the bicinchoninic acid assay and the samples were stored at −20 °C.

SPR Experiments. Silica-coated SPR chips were fabricated in house using a glass substrate coated with a 2 nm titanium adhesion layer, a 48 nm evaporated gold film, and a 4 nm silicon film deposited by plasma-enhanced chemical vapor deposition.[31] Chips were cleaned by ethanol and UV−ozone treatment before use and mounted on the flow cell of a SPR sensor from the Institute of Photonics and Electronics (Prague, Czech Republic). All experiments were conducted at a flow rate of 50 μL min^{-1} and a constant temperature of 25 °C with protein concentrations varying between 0.0312 and 1 μmol L^{-1} in 20 mM Tris-HCl at pH 7.5. Increasing the flow rate to 75 μL min^{-1} had no impact on the sigmoidicity of sfGFP−Car9 adsorption to silica, confirming kinetic control (Note 1 in Supporting Information).

Model Parameter Estimation. Initial guesses for k_{a1}, k_{d1}, k_{a2}, k_{d2}, and u (Table S1 in Supporting Information) were informed by the physical characteristics of the system and literature values. Rate constants for the first association reaction are typically on the order of 10^4 to 10^5 M^{-1} s^{-1} (classic Langmuir isotherm), while subsequent association and dissociation rate constants are in the 10^{-3} to 10^{-4} s^{-1} range based on the isotherm modeling of SPR data.[39] Bounds were adjusted in a 25% window based on initial guesses.

An objective function subject to governing equations, initial conditions, and parameter bounds was defined to minimize the mean square error (MSE) of the SPR response. With the MSE defined as the sum of the squares of differences between the model and experimental outputs divided by the total number of experimental data points, this function is expressed as

$$\text{Min } \frac{1}{N}\sum_{j=1}^{N}[R_{\text{exp},j} - R_{\text{model},j}(p)]^2 \qquad \text{s. t. } p^{\text{L}} \le p \le p^{\text{U}}$$

DOI: 10.1021/acs.langmuir.9b00283
Langmuir 2019, 35, 5013−5020

where N is the total number of experimental data points for the adsorption and desorption phases, $R_{exp,j}$ is the experimental signal value for the jth data point, $R_{model,j}(p)$ is the model-predicted value for the same point, p is the vector of estimating parameters, and p^L and p^U are its lower and upper bounds. To account for the large difference in the magnitude of the rate constants and perform a more accurate iterative optimization, the reference rate constant of the first association (k^{a1}) was scaled by 10^5 while the other rate constants were expressed as an exponent of 10 (i.e., $k_{d1} = 10^{-k}{}_{d1}$, $k_{a2} = 10^{-k}{}_{a2}$, and $k_{d2} = 10^{-k}{}_{d2}$). Initial guesses, bounds, and converged parameters are summarized in Table S1 with values rounded to three decimal places. Simulations and optimizations were carried out on a workstation with dual 8-core, 3.10 GHz Intel Xeon processors, and 32.0 GB RAM using the NLPsolve (optimization method: nonlinear simplex, and evaluation limit: maximum) in the optimization package of the Maple software.

RESULTS AND DISCUSSION

Car9 SBP Confers Proteins to Which It Is Fused Distinct Sigmoidal Adsorption Kinetics on Silica. Silica (SiO_2) surfaces are terminated with siloxanes (O−Si−O) and silanol (Si−OH) groups which can be found as isolated silanols (≡Si−OH), geminal silanols (=Si(OH)$_2$), or vicinal silanols (two H-bonded silanol groups) at distributions and with concentrations that are modulated by the synthesis method and surface ionization state.[40] Proteins that bind to silica in a nonspecific fashion do so via electrostatic and H-bonding interactions with silanol groups and hydrophobic interactions with siloxane groups.[41] Although the same interactions control the adhesion of naturally occurring and combinatorially selected silica-binding proteins and peptides to SiO_2, they are clearly deployed in a specific fashion.[42−44]

To better understand the molecular mechanisms that underpin the interaction of the Car9 SBP with silica surfaces, we quantified the binding kinetics of the sfGFP−Car9 fusion protein[37] using a gold SPR chip coated with a thin layer of SiO_2. Under conditions where wild-type sfGFP has little affinity for silica (Figure S1 in Supporting Information), all sensorgrams displayed a sigmoidal adsorption behavior typical of a cooperative process (Figure 1a). Indeed, the kinetics of the adsorption phase were poorly captured by a rate law-based 1:1 Langmuir binding model which assumes a homogeneous surface, identical binding sites, monolayer coverage, and no interactions between adsorbate molecules on adjacent sites (Figure 1b, dashed lines).[45]

Car9 contains five basic amino acids whose positively charged sidechains might contact the negatively charged silica surface. To probe the role of these interactions in the nonstandard adsorption behavior, we constructed a Car9 variant called Car9Q4 in which Lys-7, Lys-8, Lys-11, and Arg-12 were converted to uncharged glutamines. To our surprise, the sfGFP−Car9Q4 fusion protein remained functional for silica binding and could be purified by silica affinity chromatography (Figure S2 in Supporting Information). However, its affinity for the material was drastically reduced, the sensorgrams lost their sigmoidal character, and it was possible to accurately capture adsorption kinetics with a rate-based Langmuir fit (Figure 1c; also see Figure S8 in Supporting Information). We conclude that, as with the silaffin-derived R5 peptide[46,47] and other combinatorially-selected silica-binding peptides,[42] basic residues play a key role in high-affinity binding to silica. For Car9, they are also critical in determining cooperative adsorption.

To rule out the possibility that sigmoidal adsorption is driven by green fluorescent protein (GFP) dimerization events,[38] and to explore the contribution of the fused protein framework, we appended Car9 to the C-terminus of the red fluorescent protein mCherry and purified the resulting fusion by silica affinity chromatography (Figure S2 in Supporting Information). Figure 1d shows that mCherry−Car9 followed similar sigmoidal kinetics. However, saturation coverage at equimolar protein concentration was about 20−30% lower for mCherry−Car9 compared to sfGFP−Car9 in spite of the fact that the two proteins have comparable molar masses, pIs, and architectures (Figure S3 in Supporting Information; see below for a discussion).

In an effort to further generalize results, we fused Car9 to the C-terminus of a predicted glucose kinase (GK) whose gene was amplified from the genome of *Geobacillus stearothermophilus*. To our knowledge, this enzyme has not previously been expressed, and because bacterial GKs can be monomeric, dimeric, or tetrameric,[48] its quaternary structure is unknown. Thus, GK−Car9 provides an unbiased platform to test the influence of both the Car9 SBP and framework oligomeric status on silica adhesion.

We found that GK−Car9 expressed well in *E. coli* and that it could be purified to near homogeneity by silica affinity chromatography (Figure S2 in Supporting Information). Native polyacrylamide gel analysis further revealed that, like *T. thermophilus* GK,[49] *G. stearothermophilus* glucokinase forms a homotetramer (Figure 2a). A BLAST alignment revealed that the two proteins share 58% homology and 40% identity at the amino acid level (Figure S4a in Supporting Information), allowing us to model the structure of the *G. stearothermophilus* tetramer using SWISS-MODEL[50] and the *T. thermophilus* GK coordinates[49] (Figures S4b and S5 in Supporting Information). This exercise revealed that the C-termini are solvent-accessible and located in the projecting lobes of each protomer (Figure 2b).

SPR sensorgrams collected with GK−Car9 exhibited the characteristic sigmoidal adsorption behavior of Car9 fusions. Surface saturation was lower than with either sfGFP−Car9 or mCherry−Car9 (Figure 2c). Thus, at least when carboxyl termini are accessible, the oligomerization status of the fusion partner does not affect the cooperative nature of binding. To summarize, the Car9 SBP drives high-affinity binding to silica through a unique cooperative adsorption process that relies on the presence of basic residues but is independent of the identity and oligomeric status of the fused protein scaffold.

Modeling the Kinetics of Car9−Silica Interactions. To model the sigmoidal character of Car9-mediated adsorption kinetics, we developed a rate law expression based on the Frumkin−Fowler−Guggenheim isotherm,[51] which takes into consideration attractive or repulsive lateral interactions between neighboring adsorbate molecules and reduces to the Langmuir formalism when these interactions are absent.[52,53] Furthermore, because the kinetics of the desorption phase are poorly captured by a single exponential decay (Figure S6 in Supporting Information), we included a second reaction step that can be conceptualized as a change in the conformation of the SBP once initial adsorption and nearest neighbor contacts have occurred at the silica interface. Diffusional limitations were neglected as justified in Note 1 in the Supporting Information. A schematic depiction of this process and the governing equations of the resulting two-step model are presented in Figure 3.

DOI: 10.1021/acs.langmuir.9b00283
Langmuir 2019, 35, 5013−5020

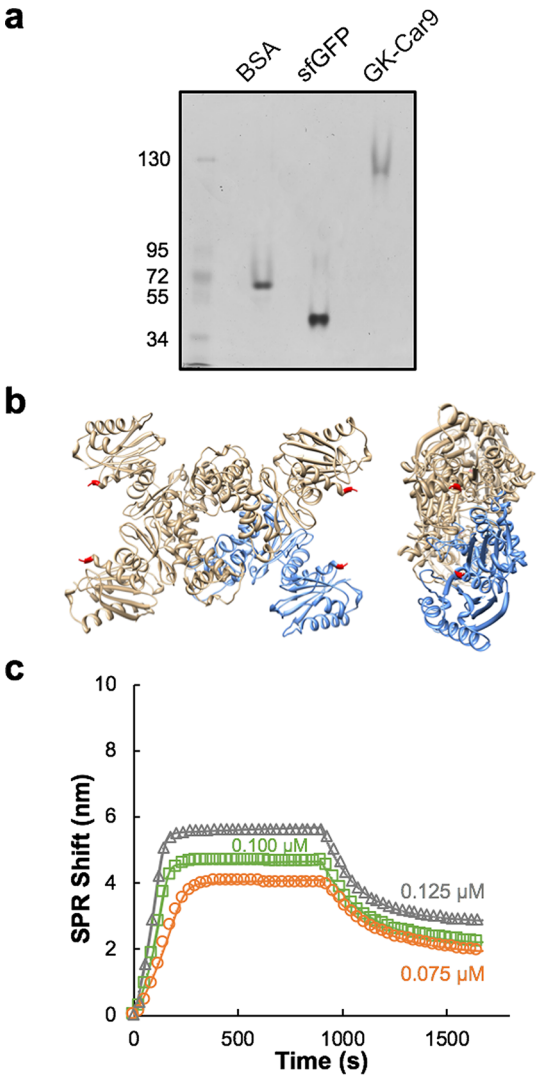

Figure 2. Oligomerization, predicted structure, and silica-binding properties of GK−Car9. (a) Native polyacrylamide gel analysis of GK−Car9 showing the migration positions of marker proteins and those of bovine serum albumin (66 kDa) and sfGFP (26.8 kDa). (b) Predicted quaternary structure of the GK oligomer. In these front and side views, a monomer is shown in blue and the four C-termini are colored in red. (c) Adsorption kinetics of GK−Car9 on silica-coated SPR chips. Fits obtained with the two-step cooperative adsorption model are shown with solid lines.

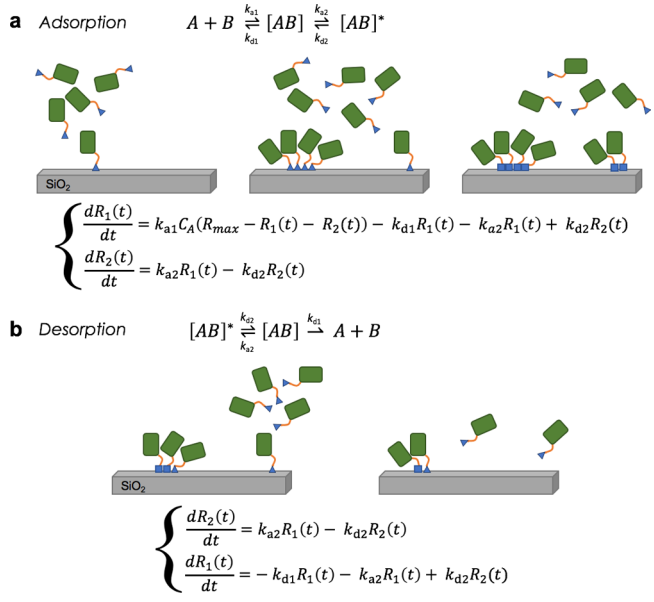

Figure 3. Proposed two-step cooperative binding model for the adsorption of Car9 fusion proteins to silica surfaces. The adsorption and desorption phases are schematically illustrated with proteins depicted in green, linkers in orange, and Car9 SBPs as blue triangles or blue squares to reflect the fact that they undergo a conformational change after they have bound to the silica surface. (A similar conformation change occurs upon desorption). The governing equations which are simultaneously solved by the optimization routine are also shown. $R_1(t)$ and $R_2(t)$ correspond to the time-dependent SPR responses associated with the first and second adsorption/desorption phases, respectively. The Car9 SBP drives protein adsorption to the silica surface (a) at a rate dependent on the rate constant k_{a1}, the bulk protein concentration C_A, and the surface concentration of free binding sites. Interactions between neighboring Car9 moieties, and to a lesser extent between fused protein frameworks, engender a cooperative behavior. Bound species next undergo a conformational rearrangement at the interface or desorb from the surface. These are parallel first-order processes with rate constants k_{d1} and k_{a2}. The isomerization step is reversible, and the bound forms corresponding to signal $R_2(t)$ can convert back to the original isomeric form with first-order kinetics and a rate constant k_{d2}. The desorption phase (b) is described by the absence of analyte in the bulk liquid, ($C_A = 0$). Adsorbed proteins switch between isomeric forms, with parallel desorption of the isomer corresponding to signal $R_1(t)$ back into the liquid phase. This causes the gradual decay in SPR signals observed in the desorption phase of the SPR sensorgrams. See Note 2 in the Supporting Information for a detailed explanation of model equations.

The rate law expression for the initial adsorption step considers the product of the flux and a sticking probability which depends on the lateral interaction energy between adsorbed species. The equivalent rate constant for adsorption (k_{a1} in Table 1) is thus expressed as

$$k_{a1} = \frac{N_A}{\sigma_{max}}\sqrt{\frac{RT}{2\pi M}}\exp\left(\frac{-E_0}{RT}\right)\exp\left(\frac{-E_i\theta}{RT}\right) \quad (1)$$

where N_A is Avogadro's number, σ_{max} is the density of binding sites on the silica surface which is assumed to be identical under prescribed solution conditions, M is the molar mass of the adsorbing protein, R is the universal gas constant, E_0 is the molar intrinsic activation energy for bond formation between SBP and surface, and E_i is the molar interaction energy between nearest neighbors, a quantity that is negative for attractive interactions. We assume that the time-dependent SPR responses $R_1(t)$ and $R_2(t)$ are directly proportional to protein surface concentrations. This allows us to take θ, the surface coverage at time t, to be proportional to the ratio of the sum of the SPR signals in each adsorption phase divided by R_{max}, the maximum SPR signal at saturation

$$\theta \propto \frac{R_1(t) + R_2(t)}{R_{max}} \quad (2)$$

At fixed temperature T, and for a given solid-binding protein and concentration of binding sites on the silica surface, the species and temperature-dependent properties in eq 1 can be combined into a single parameter to give a rate constant of the form

$$k_{a1} = k'_{a1}\exp(u\theta) \quad (3)$$

DOI: 10.1021/acs.langmuir.9b00283
Langmuir 2019, 35, 5013−5020

Table 1. Kinetic Parameters for the Two-Step Adsorption of Car9 Fusion Proteins at pH 7.5

protein[a]	[NaCl] (M)	u	k'_{a1} (M^{-1} s^{-1})	$k_{d1} \times 10^{-3}$ (s^{-1})	$k_{a2} \times 10^{-3}$ (s^{-1})	$k_{d2} \times 10^{-3}$ (s^{-1})
sfGFP−Car9[a]	0	2.9 ± 0.1	20 700 ± 1200	0.76 ± 0.05	0.17 ± 0.05	0.03 ± 0.01
mCherry−Car9[a]	0	2.9 ± 0.1	27 100 ± 1200	2.40 ± 0.60	0.85 ± 0.20	0.20 ± 0.10
GK−Car9[a]	0	3.1 ± 0.2	34 100 ± 900	4.32 ± 0.90	0.67 ± 0.10	0.05 ± 0.01
sfGFP−Car9[b]	0	2.9	20 000	0.84	0.12	0.060
sfGFP−Car9[b]	0.05	2.2	29 000	2.15	0.20	0.020
sfGFP−Car9[b]	0.1	2.3	30 000	4.71	0.51	0.100

[a]Mean and standard deviations were obtained from three fits of SPR data obtained on the same chip at protein concentrations of 0.031, 0.075, and 0.1 μM for sfGFP−Car9, 0.05, 0.075, and 0.1 μM for mCherry−Car9, and 0.075, 0.1, and 0.125 μM for GK−Car9. [b]Model parameters were extracted from the experimental data of Figure 4, which was conducted on a single chip and at a sfGFP−Car9 concentration of 0.125 μM with the indicated concentrations of NaCl.

where

$$k'_{a1}(T) = \frac{N_A}{\sigma_{max}}\sqrt{\frac{RT}{2\pi M}}\exp\left(\frac{-E_0}{RT}\right) \quad (4)$$

and

$$u(T) = \frac{-E_i}{RT} \quad (5)$$

Thus, the entirety of protein−surface interactions is accounted for by the modified rate constant k'_{a1}. Of note, the overall rate constant k_{a1} also depends on the concentration of binding sites available on the surface through the exponential factor $\exp(u\theta)$ which changes with surface coverage. This factor accounts for cooperative SBP−SBP interactions and framework contributions. A detailed derivation of the governing equations can be found in Note 2 in the Supporting Information.

Model Validation. The solid lines in Figure 1a show that the proposed model closely fits the experimental data and that it accurately captures the distinct sigmoidal adsorption phase of sfGFP−Car9 on silica. Desorption kinetics, which are simultaneously fit by the optimization routine, are also captured with good fidelity. However, the match with experimental data is not as good presumably because our model does not account for protein readsorption events. Examination of extracted parameters for sfGFP−Car9 (Table 1) reveals that the first adsorption step is kinetically dominant and that it occurs with positive cooperativity ($u > 0$), firmly implicating protein−protein interactions in high-affinity silica binding. The second step—an isomerization reaction—occurs with significantly slower kinetics (Table 1), as confirmed in Figure S7 in the Supporting Information by a comparison of the simulated values of instantaneous adsorption and desorption rates for each reaction.

Our observation that sfGFP−Car9, mCherry−Car9, and GK−Car9 adsorb to silica with comparable u values (Table 1) indicates that interactions between nearest neighbor Car9 segments are the main driver for cooperativity and that framework−framework interactions only play a minor role in the process. The slight (~15%) increase in the value of u for GK−Car9 is not unexpected and consistent with a situation in which copresentation of four SBPs per GK−Car9 oligomer increases the likelihood of lateral interactions with Car9 segments from neighboring tetramers.

Table 1 further shows that both mCherry−Car9 and GK−Car9 adsorb to silica with a higher k'_{a1} than sfGFP−Car9. In the case of GK−Car9, this result is well explained by the fact that four Car9 extensions per GK oligomer are more effective at reducing the energy barrier E_0 than a single SBP because they contribute combined attractive electrostatic interactions between the protein and surface. The associated increase in k'_{a1} clearly dominates over the opposite effect brought about by the higher molar mass of GK−Car9 protomers (34.2 kDa compared to 28.6 kDa for sfGFP−Car9 monomers; see eq 4). In the case of mCherry−Car9, a monomeric protein comparable in mass and shape to sfGFP−Car9, the increase in k'_{a1} likely results from more subtle framework effects. For instance, the "bottom" face of mCherry from which the Car9 extension projects has a higher electrostatic potential than the bottom face of sfGFP (Figure S3 in Supporting Information). This might minimize short-range electrostatic interactions between the mCherry framework and the positively charged SBP, allowing Car9 to more efficiently engage the silica surface.

It is finally of interest to note that both mCherry−Car9 and GK−Car9 desorb at higher rates than sfGFP−Car9 after initial adsorption. The higher k_{d1} values, along with a more complex interplay of association and dissociation events during the isomerization step, account for the lower saturation coverage (e.g., compare Figures 1a,d and 2c at 0.1 μM). For comparison, the fitting of sfGFP−Car9Q4 sensorgram data with a rate law-based Langmuir model that is appropriate for the dataset (Figures 1c and S8 in Supporting Information) yields values of k_a (3000 ± 100 M^{-1} s^{-1}) and k_d ($0.18 \times 10^{-3} \pm 0.07 \times 10^{-3}$ s^{-1}) that are typical of nonspecific protein adsorption processes.[54]

Influence of Ionic Strength. To assess the robustness of our model, we conducted additional SPR experiments using 0.125 μM sfGFP−Car9 and increasing concentrations of sodium chloride to screen charges on both the silica surface and protein shell. All sensorgrams retained a sigmoidal character, establishing the validity of the cooperative two-step model under more physiological solution conditions (Figure 4). However, there was a ~40% decrease in saturation surface coverage in the presence of 50 mM of NaCl and an additional 10% decrease in θ at 100 mM of NaCl. These results can be explained by the screening of silanol-rich Car9 binding sites by sodium ions, and they are consistent with the observation that the zeta potential of silica nanoparticles decreases from −55 to −27 mV when the NaCl concentration is increased from 0 to 100 mM at neutral pH.[55]

Parameters extracted from the model provide validation for the above hypothesis and insights into the molecular basis of ionic effects (Table 1). First, a decrease in the net number of Car9 binding sites (captured by parameter σ_{max} in eq 4) should cause k'_{a1} to increase with the salt concentration, a behavior that we observe experimentally. NaCl may also contribute to the increase in k'_{a1} by shielding repulsive interactions between the sfGFP framework and silica surface, thus reducing the

DOI: 10.1021/acs.langmuir.9b00283
Langmuir 2019, 35, 5013−5020

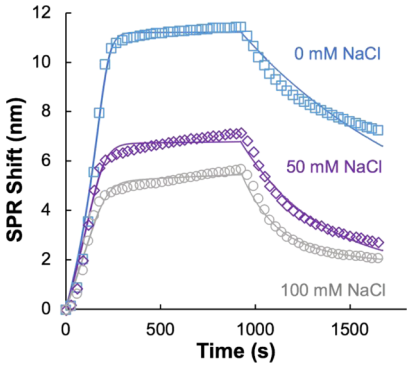

Figure 4. Influence of the NaCl concentration on the adsorption of sfGFP−Car9 (0.125 μM) to silica substrates.

activation barrier E_0. Second, there is a 25% decline in the value of u in the presence of salt. This suggests that attractive electrostatic interactions between neighboring Car9 domains (and to a lower extent sfGFP monomers, see above) contribute to cooperativity and are shielded in the presence of salt. Third, the increase in the rate of protein desorption (k_{d1}) with salt concentration is consistent with such weakened lateral interaction and a lower protein coverage, much likely we observe with GK−Car9. Finally, there is a progressive increase in the rate constant for the isomerization step (k_{a2}) with salt concentration (Table 1). While the underlying mechanism remains unclear, it is tempting to hypothesize that the ionic screening of lysine, arginine, and aspartate side chains facilitates conformational rearrangement of Car9 extensions at the silica interface.

SUMMARY AND CONCLUSIONS

SPR[23,24] and QCM[56] are mature characterization techniques that have proven remarkably useful for quantifying the binding of biomacromolecules to ligands immobilized on sensor chips. They have also been used for well over a decade to study the direct interaction of SBPs with inorganic and synthetic surfaces.[3,21] In most cases, adsorption isotherms are treated with a 1:1 Langmuir model and kinetic parameters and free energies of binding are extracted from the fit. At the exception of a handful of studies by Sarikaya and co-workers[21,27−29] in which a biexponential Langmuir model was used to capture nonideality in the binding of gold-binding peptides—a phenomenon originally thought to be associated with the polycrystalline nature of the surface but later attributed to surface diffusivity and time-dependent evolution of adsorbed peptide structures[30]—little attention has been paid to the appropriateness of the Langmuir treatment.[57] The fact that QCM and SPR measurements are often noisy when conducted at low concentrations of synthetic peptides further complicates the recognition that a SBP adsorption process might not obey Langmuir kinetics.

Here, we have used large fusion proteins to characterize the adsorption of the promiscuous and technologically useful Car9 peptide to silica-coated SPR chips. The approach yields high-quality sensorgrams and enables SBP compositional and functional analysis within a solubilizing context. Of relevance to our long-term goal of installing SBPs within computationally designed scaffolds for the controlled assembly of hierarchical structures, it also provides molecular insights into how SBP, surface, fusion partner, and solution conditions modulate binding.

Our results indicate that Car9 endows protein scaffolds to which it is fused with a sigmoidal adsorption behavior on silica, irrespective of—but influenced by—the identity of the host framework and the SBP valency. This unique adsorption modality was accurately captured by a two-step kinetic reaction model in which cooperative binding driven by intermolecular contacts between Car9 extensions (and to a lesser extent by fused framework contributions) is followed by an isomerization step that "locks" SBP and fusion partner in a high-affinity interaction with the surface. The model is consistent with both the tendency of certain SBPs to self-assemble into ordered structures at interfaces,[14,20,30,58] and with the enthalpic binding mechanism proposed by Walsh and Knecht[3,59,60] in which anchor residues (amino acids that spend a significant amount of time at the interface) mediate strong enthalpic contacts between SBP and silica. By contrast, sfGFP−Car9Q4 exhibits a more traditional Langmuir behavior. It may, therefore, belong to the class of entropic SBPs which achieve high-affinity binding by assuming multiple conformations at the interface.[3,59,60] Such a conversion in binding modalities between Car9 isoforms suggests that it should be possible to gain a detailed understanding of how Car9 adsorbs to silica by generating a panel of Car9 mutants, pairing model parameter extraction from SPR experiments with structural predictions and advanced molecular dynamics simulations.

The approach described herein should be generalizable to other technologically useful SBPs exhibiting non-Langmuir adsorption. It should also provide a rich source of information on how SBP−SBP interactions, host framework, and solution conditions modulate adhesion, which will be critical in enabling predictive material synthesis with solid-binding proteins.

ASSOCIATED CONTENT

Supporting Information

The Supporting Information is available free of charge on the ACS Publications website at DOI: 10.1021/acs.langmuir.9b00283.

Adsorption kinetics of sfGFP on silica-coated SPR chips, purification and silica-binding activity of proteins used in this study, electrostatic surface of sfGFP and mCherry, alignment and homology model of *G. stearothermophilus* glucose kinase based on the sequence and crystal structure coordinates of *T. thermophilus* glucose kinase, electrostatic surface of *G. stearothermophilus* glucose kinase, desorption kinetics of sfGFP−Car9 modeled with a single exponential decay or the two-step cooperative model, simulated instantaneous reaction rates of sfGFP−Car9 adsorption and desorption, summary of lower and upper bounds, and initial guesses for the fitting of sigmoidal sensorgrams using the proposed two step model, justifying the assumption of kinetic control and derivation of model equations (PDF)

AUTHOR INFORMATION

Corresponding Author

*E-mail: baneyx@uw.edu.

ORCID

François Baneyx: 0000-0001-5596-7903

Notes

The authors declare the following competing financial interest(s): F.B. declares competing financial interest in

DOI: 10.1021/acs.langmuir.9b00283
Langmuir 2019, 35, 5013−5020

Proteios which researches and commercializes Car9-based technologies.

■ ACKNOWLEDGMENTS

This material is based upon work supported by the US Department of Energy, Office of Science, Office of Basic Energy Sciences, as part of the Energy Frontier Research Centers program: CSSAS, The Center for the Science of Synthesis Across Scales under Award Number DE-SC0019288. SPR chips were fabricated at the Washington Nanofabrication Facility, a member of the National Nanotechnology Coordinated Infrastructure (NNCI). We thank Dr. Meng Xu for cloning the GK gene.

■ REFERENCES

(1) Dickerson, M. B.; Sandhage, K. H.; Naik, R. R. Protein- and Peptide-Directed Syntheses of Inorganic Materials. *Chem. Rev.* **2008**, *108*, 4935−4978.
(2) Sarikaya, M.; Tamerler, C.; Schwartz, D. T.; Baneyx, F. Materials assembly and formation using engineered polypeptides. *Annu. Rev. Mater. Res.* **2004**, *34*, 373−408.
(3) Walsh, T. R.; Knecht, M. R. Biointerface structural effects on the properties and applications of bioinspired peptide-based nanomaterials. *Chem. Rev.* **2017**, *117*, 12641−12704.
(4) Kashiwagi, K.; Tsuji, T.; Shiba, K. Directional bmp-2 for functionalization of titanium surfaces. *Biomaterials* **2009**, *30*, 1166−1175.
(5) Mieszawska, A. J.; Nadkarni, L. D.; Perry, C. C.; Kaplan, D. L. Nanoscale Control of Silica Particle Formation via Silk−Silica Fusion Proteins for Bone Regeneration. *Chem. Mater.* **2010**, *22*, 5780−5785.
(6) Huang, Z. B.; Shi, X.; Mao, J.; Gong, S. Q. Design of a hydroxyapatite-binding antimicrobial peptide with improved retention and antibacterial efficacy for oral pathogen control. *Sci. Rep.* **2016**, *6*, 38410.
(7) Yi, H.; Ghosh, D.; Ham, M.-H.; Qi, J.; Barone, P. W.; Strano, M. S.; Belcher, A. M. M13 phage-functionalized single-walled carbon nanotubes as nanoprobes for second near-infrared window fluorescence imaging of targeted tumors. *Nano Lett.* **2012**, *12*, 1176−1183.
(8) Bedford, N. M.; Hughes, Z. E.; Tang, Z.; Li, Y.; Briggs, B. D.; Ren, Y.; Swihart, M. T.; Petkov, V. G.; Naik, R. R.; Knecht, M. R.; Walsh, T. R. Sequence-Dependent Structure/Function Relationships of Catalytic Peptide-Enabled Gold Nanoparticles Generated under Ambient Synthetic Conditions. *J Am Chem Soc* **2016**, *138*, 540.
(9) Bedford, N. M.; Ramezani-Dakhel, H.; Slocik, J. M.; Briggs, B. D.; Ren, Y.; Frenkel, A. I.; Petkov, V.; Heinz, H.; Naik, R. R.; Knecht, M. R. Elucidation of peptide-directed palladium surface structure for biologically tunable nanocatalysts. *ACS Nano* **2015**, *9*, 5082−5092.
(10) Lee, Y. J.; Yi, H.; Kim, W. J.; Kang, K.; Yun, D. S.; Strano, M. S.; Ceder, G.; Belcher, A. M. Fabricating genetically engineered high-power lithium-ion batteries using multiple virus genes. *Science* **2009**, *324*, 1051−1055.
(11) Oh, D.; Qi, J.; Lu, Y. C.; Zhang, Y.; Shao-Horn, Y.; Belcher, A. M. Biologically enhanced cathode design for improved capacity and cycle life for lithium-oxygen batteries. *Nat. Commun.* **2013**, *4*, 2756.
(12) Nam, Y. S.; Magyar, A. P.; Lee, D.; Kim, J.-W.; Yun, D. S.; Park, H.; Pollom, T. S., Jr.; Weitz, D. A.; Belcher, A. M. Biologically templated photocatalytic nanostructures for sustained light-driven water oxidation. *Nat. Nanotechnol.* **2010**, *5*, 340−344.
(13) Soto-Rodríguez, J.; Hemmatian, Z.; Josberger, E. E.; Rolandi, M.; Baneyx, F. A palladium-binding deltarhodopsin for light-activated conversion of protonic to electronic currents. *Adv. Mater.* **2016**, *28*, 6581−6585.
(14) Hayamizu, Y.; So, C. R.; Dag, S.; Page, T. S.; Starkebaum, D.; Sarikaya, M. Bioelectronic interfaces by spontaneously organized peptides on 2d atomic single layer materials. *Sci. Rep.* **2016**, *6*, 33778.
(15) Chen, H.; Su, X.; Neoh, K.-G.; Choe, W.-S. QCM-D Analysis of Binding Mechanism of Phage Particles Displaying a Constrained Heptapeptide with Specific Affinity to SiO2and TiO2. *Anal. Chem.* **2006**, *78*, 4872−4879.
(16) Phillips, D. C.; York, R. L.; Mermut, O.; McCrea, K. R.; Ward, R. S.; Somorjai, G. A. Side chain, chain length, and sequence effects on amphiphilic peptide adsorption at hydrophobic and hydrophilic surfaces studied by sum-frequency generation vibrational spectroscopy and quartz crystal microbalance. *J. Phys. Chem. C* **2007**, *111*, 255−261.
(17) Weidner, T.; Breen, N. F.; Li, K.; Drobny, G. P.; Castner, D. G. Sum frequency generation and solid-state nmr study of the structure, orientation, and dynamics of polystyrene-adsorbed peptides. *Proc. Natl. Acad. Sci. U.S.A.* **2010**, *107*, 13288−13293.
(18) Thyparambil, A. A.; Wei, Y.; Latour, R. A. Determination of Peptide-Surface Adsorption Free Energy for Material Surfaces Not Conducive to SPR or QCM using AFM. *Langmuir* **2012**, *28*, 5687−5694.
(19) Russo, C. J.; Passmore, L. A. Controlling protein adsorption on graphene for cryo-em using low-energy hydrogen plasmas. *Nat. Methods* **2014**, *11*, 649−652.
(20) Chen, J.; Zhu, E.; Liu, J.; Zhang, S.; Lin, Z.; Duan, X.; Heinz, H.; Huang, Y.; De Yoreo, J. J. Building two-dimensional materials one row at a time: Avoiding the nucleation barrier. *Science* **2018**, *362*, 1135−1139.
(21) Tamerler, C.; Oren, E. E.; Duman, M.; Venkatasubramanian, E.; Sarikaya, M. Adsorption kinetics of an engineered gold binding peptide by surface plasmon resonance spectroscopy and a quartz crystal microbalance. *Langmuir* **2006**, *22*, 7712−7718.
(22) Nergiz, S. Z.; Slocik, J. M.; Naik, R. R.; Singamaneni, S. Surface defect sites facilitate fibrillation: An insight into adsorption of gold-binding peptides on au(111). *Phys. Chem. Chem. Phys.* **2013**, *15*, 11629−11633.
(23) Guo, X. Surface plasmon resonance based biosensor technique: A review. *J. Biophotonics* **2012**, *5*, 483−501.
(24) Homola, J. Surface plasmon resonance sensors for detection of chemical and biological species. *Chem. Rev.* **2008**, *108*, 462−493.
(25) Green, R. J.; Frazier, R. A.; Shakesheff, K. M.; Davies, M. C.; Roberts, C. J.; Tendler, S. J. B. Surface plasmon resonance analysis of dynamic biological interactions with biomaterials. *Biomaterials* **2000**, *21*, 1823−1835.
(26) Hnilova, M.; Oren, E. E.; Seker, U. O. S.; Wilson, B. R.; Collino, S.; Evans, J. S.; Tamerler, C.; Sarikaya, M. Effect of molecular conformations on the adsorption behavior of gold-binding peptides. *Langmuir* **2008**, *24*, 12440−12445.
(27) Seker, U. O. S.; Wilson, B.; Kulp, J. L.; Evans, J. S.; Tamerler, C.; Sarikaya, M. Thermodynamics of engineered gold binding peptides: Establishing the structure-activity relationships. *Biomacromolecules* **2014**, *15*, 2369−2377.
(28) Seker, U. O. S.; Wilson, B.; Dincer, S.; Kim, I. W.; Oren, E. E.; Evans, J. S.; Tamerler, C.; Sarikaya, M. Adsorption behavior of linear and cyclic genetically engineered platinum binding peptides. *Langmuir* **2007**, *23*, 7895−7900.
(29) Seker, U. O. S.; Wilson, B.; Sahin, D.; Tamerler, C.; Sarikaya, M. Quantitative affinity of genetically engineered repeating polypeptides to inorganic surfaces. *Biomacromolecules* **2009**, *10*, 250−257.
(30) So, C. R.; Tamerler, C.; Sarikaya, M. Adsorption, diffusion, and self-assembly of an engineered gold-binding peptide on au(111) investigated by atomic force microscopy. *Angew. Chem., Int. Ed.* **2009**, *48*, 5174−5177.
(31) Coyle, B. L.; Rolandi, M.; Baneyx, F. Carbon-binding designer proteins that discriminate between sp2- and sp3-hybridized carbon surfaces. *Langmuir* **2013**, *29*, 4839−4846.
(32) Karlsson, R.; Fält, A. Experimental design for kinetic analysis of protein-protein interactions with surface plasmon resonance biosensors. *J. Immunol. Methods* **1997**, *200*, 121−133.
(33) Coyle, B. L.; Baneyx, F. A cleavable silica-binding affinity tag for rapid and inexpensive protein purification. *Biotechnol. Bioeng.* **2014**, *111*, 2019−2026.

DOI: 10.1021/acs.langmuir.9b00283
Langmuir 2019, 35, 5013−5020

(34) Swift, B. J. F.; Shadish, J. A.; DeForest, C. A.; Baneyx, F. Streamlined synthesis and assembly of a hybrid sensing architecture with solid binding proteins and click chemistry. *J. Am. Chem. Soc.* **2017**, *139*, 3958−3961.
(35) Soto-Rodríguez, J.; Coyle, B. L.; Samuelson, A.; Aravagiri, K.; Baneyx, F. Affinity purification of car9-tagged proteins on silica matrices: Optimization of a rapid and inexpensive protein purification technology. *Protein Expression Purif.* **2017**, *135*, 70−77.
(36) Yang, W.; Hellner, B.; Baneyx, F. Self-immobilization of car9 fusion proteins within high surface area silica sol-gels and dynamic control of protein release. *Bioconjugate Chem.* **2016**, *27*, 2450−2459.
(37) Coyle, B. L.; Baneyx, F. Direct and reversible immobilization and microcontact printing of functional proteins on glass using a genetically appended silica-binding tag. *Chem. Commun.* **2016**, *52*, 7001−7004.
(38) Pédelacq, J.-D.; Cabantous, S.; Tran, T.; Terwilliger, T. C.; Waldo, G. S. Engineering and characterization of a superfolder green fluorescent protein. *Nat. Biotechnol.* **2006**, *24*, 79−88.
(39) Morton, T. A.; Myszka, D. G.; Chaiken, I. M. Interpreting complex binding kinetics from optical biosensors: A comparison of analysis by linearization, the integrated rate equation, and numerical integration. *Anal. Biochem.* **1995**, *227*, 176−185.
(40) Parida, S. K.; Dash, S.; Patel, S.; Mishra, B. K. Adsorption of organic molecules on silica surface. *Adv. Colloid Interface Sci.* **2006**, *121*, 77−110.
(41) Ghose, S.; McNerney, T. M.; Hubbard, B. Preparative protein purification on underivatized silica. *Biotechnol. Bioeng.* **2004**, *87*, 413−423.
(42) Patwardhan, S. V.; Emami, F. S.; Berry, R. J.; Jones, S. E.; Naik, R. R.; Deschaume, O.; Heinz, H.; Perry, C. C. Chemistry of aqueous silica nanoparticle surfaces and the mechanism of selective peptide adsorption. *J. Am. Chem. Soc.* **2012**, *134*, 6244−6256.
(43) Puddu, V.; Perry, C. C. Peptide adsorption on silica nanoparticles: Evidence of hydrophobic interactions. *ACS Nano* **2012**, *6*, 6356−6363.
(44) Puddu, V.; Perry, C. C. Interactions at the silica-peptide interface: The influence of particle size and surface functionality. *Langmuir* **2014**, *30*, 227−233.
(45) Lan, Q.; Bassi, A. S.; Zhu, J.-X.; Margaritis, A. A modified langmuir model for the prediction of the effects of ionic strength on the equilibrium characteristics of protein adsorption onto ion exchange/affinity adsorbents. *Chem. Eng. J.* **2001**, *81*, 179−186.
(46) Knecht, M. R.; Wright, D. W. Functional analysis of the biomimetic silica precipitating activity of the R5 peptide from Cylindrotheca fusiformisElectronic supplementary information (ESI) available: HPLC and MALDI of peptides (11 pgs); EMs of silica particles (4 pgs); IR data (3 pgs); DLS data (1 pg) and mechanistic detail (1 pg). See http://www.rsc.org/suppdata/cc/b3/b309074d/. *Chem. Commun.* **2003**, 3038−3039.
(47) Lechner, C. C.; Becker, C. F. W. A sequence-function analysis of the silica precipitating silaffin r5 peptide. *J. Pept. Sci.* **2014**, *20*, 152−158.
(48) Romero-Rodríguez, A.; Ruiz-Villafán, B.; Rocha-Mendoza, D.; Manzo-Ruiz, M.; Sánchez, S. Biochemistry and regulatory functions of bacterial glucose kinases. *Arch. Biochem. Biophys.* **2015**, *577*−*578*, 1−10.
(49) Nakamura, T.; Kashima, Y.; Mine, S.; Oku, T.; Uegaki, K. Characterization and crystal structure of the thermophilic rok hexokinase from thermus thermophilus. *J. Biosci. Bioeng.* **2012**, *114*, 150−154.
(50) Biasini, M.; Bienert, S.; Waterhouse, A.; Arnold, K.; Studer, G.; Schmidt, T.; Kiefer, F.; Cassarino, T. G.; Bertoni, M.; Bordoli, L.; Schwede, T. Swiss-model: Modelling protein tertiary and quaternary structure using evolutionary information. *Nucleic Acids Res.* **2014**, *42*, W252−W258.
(51) Fowler, R., Guggenheim, E. A. *Statistical Thermodynamics*; Cambridge University Press: Cambridge, United Kingdom, 1949.
(52) de Keizer, A.; Fokkink, L. G. J. Specific adsorption of organic cations at the silver iodide-electrolyte interface. *Colloids Surf.* **1990**, *51*, 323−337.
(53) Al-Abadleh, H. A.; Mifflin, A. L.; Bertin, P. A.; Nguyen, S. T.; Geiger, F. M. Control of carboxylic acid and ester groups on chromium (vi) binding to functionalized silica/water interfaces studied by second harmonic generation. *J. Phys. Chem. B* **2005**, *109*, 9691−9702.
(54) Brewer, S. H.; Glomm, W. R.; Johnson, M. C.; Knag, M. K.; Franzen, S. Probing bsa binding to citrate-coated gold nanoparticles and surfaces. *Langmuir* **2005**, *21*, 9303−9307.
(55) Meissner, J.; Prause, A.; Bharti, B.; Findenegg, G. H. Characterization of protein adsorption onto silica nanoparticles: Influence of ph and ionic strength. *Colloid Polym. Sci.* **2015**, *293*, 3381−3391.
(56) Marx, K. A. Quartz Crystal Microbalance: A Useful Tool for Studying Thin Polymer Films and Complex Biomolecular Systems at the Solution−Surface Interface. *Biomacromolecules* **2003**, *4*, 1099−1120.
(57) Latour, R. A. The langmuir isotherm: A commonly applied but misleading approach for the analysis of protein adsorption behavior. *J. Biomed. Mater. Res., Part A* **2015**, *103*, 949−958.
(58) So, C. R.; Hayamizu, Y.; Yazici, H.; Gresswell, C.; Khatayevich, D.; Tamerler, C.; Sarikaya, M. Controlling self-assembly of engineered peptides on graphite by rational mutation. *ACS Nano* **2012**, *6*, 1648−1656.
(59) Palafox-Hernandez, J. P.; Tang, Z.; Hughes, Z. E.; Li, Y.; Swihart, M. T.; Prasad, P. N.; Walsh, T. R.; Knecht, M. R. Comparative study of materials-binding peptide interactions with gold and silver surfaces and nanostructures: A thermodynamic basis for biological selectivity of inorganic materials. *Chem. Mater.* **2014**, *26*, 4960−4969.
(60) Tang, Z.; Palafox-Hernandez, J. P.; Law, W.-C.; Hughes, Z. E.; Swihart, M. T.; Prasad, P. N.; Knecht, M. R.; Walsh, T. R. Biomolecular recognition principles for bionanocombinatorics: An integrated approach to elucidate enthalpic and entropic factors. *ACS Nano* **2013**, *7*, 9632−9646.

DOI: 10.1021/acs.langmuir.9b00283
Langmuir 2019, 35, 5013−5020